

## Numerical calculation of axisymmetric electrostatic modes for cold finitlength nonneutral plasmas

Johnny K. Jennings, Ross L. Spencer, and K. C. Hansen

Citation: *Physics of Plasmas* (1994-present) **2**, 2630 (1995); doi: 10.1063/1.871228

View online: <http://dx.doi.org/10.1063/1.871228>

View Table of Contents: <http://scitation.aip.org/content/aip/journal/pop/2/7?ver=pdfcov>

Published by the [AIP Publishing](#)

---

A collection of five pieces of industrial vacuum equipment from Pfeiffer Vacuum, including a red turbopump, a silver turbopump, a white backing pump, a red leak detector, and a silver measurement chamber.

 Vacuum Solutions from a Single Source

- Turbopumps
- Backing pumps
- Leak detectors
- Measurement and analysis equipment
- Chambers and components

**PFEIFFER**  *VACUUM*

# Numerical calculation of axisymmetric electrostatic modes for cold finite-length non-neutral plasmas

Johnny K. Jennings, Ross L. Spencer, and K. C. Hansen

*Department of Physics and Astronomy, Brigham Young University, Provo, Utah 84602*

(Received 28 November 1994; accepted 20 March 1995)

A numerical calculation of mode frequencies for cold, non-neutral plasmas is reported. The numerical method can be applied to any axisymmetric plasma shape in a trap. Here, it is used to study axisymmetric electrostatic modes in a long conducting cylinder. These modes were previously studied by Prasad and O'Neil [Phys. Fluids **26**, 665 (1983)] and by Dubin [Phys. Rev. Lett. **66**, 2076 (1991)]. In contrast to Dubin's calculation, the effects of a nearby cylindrical wall, including its influence on the shape of the plasma equilibrium, are considered. It is found that for plasmas with aspect ratios (length divided by diameter) near unity the numerical results can be approximately obtained by judiciously combining Dubin's calculation, and the Trivelpiece-Gould dispersion relation for infinitely-long geometry. For aspect ratios larger than about three, the Trivelpiece-Gould dispersion relation can be used in a simple way to obtain the numerically-computed mode frequencies with an accuracy of 1%, or better. The potential use of this calculation as a plasma diagnostic is also discussed, and it is argued that at the present level of accuracy (1–2%) its usefulness is marginal, but that an improvement by an order of magnitude might make it more interesting. © 1995 American Institute of Physics.

## I. INTRODUCTION

Plasmas consist of many charged particles whose interactions are dominated by collective effects. Non-neutral plasmas are also dominated by collective effects, but do not satisfy the usual requirement that plasmas be quasineutral. An example of a non-neutral plasma is the pure electron plasma, which has been studied extensively by Malmberg and coworkers.<sup>1</sup> Much of what is known about non-neutral plasmas is discussed in Davidson.<sup>2</sup>

The modes of oscillation of non-neutral plasmas are interesting, both in their own right and also because of their potential as non-destructive diagnostics.<sup>3,4</sup> They are only useful in this way, however, if it is possible accurately to calculate mode frequencies for confinement geometries and plasmas of interest. The simplest calculation of the mode frequencies of such plasmas is in infinitely-long geometry with constant plasma density inside the plasma radius  $r_p$ , with uniform magnetic field, and with zero temperature, where the Trivelpiece-Gould dispersion relation is obtained.<sup>5</sup> The effects of finite-length were approximately treated by Prasad and O'Neil<sup>6</sup> for long, cylindrically-shaped plasmas in cylindrical traps, but without including the effects of realistic equilibrium shapes. Dubin<sup>7</sup> solved the electrostatic fluid mode equation for cold plasmas of spheroidal equilibrium shape (with the conducting walls infinitely far away). We solve numerically for axisymmetric electrostatic modes in cold plasmas with a uniform magnetic field, including the effects of a conducting cylinder and of the correct equilibrium shape. Although the discussion in this paper is limited to the effects of cylindrical conducting walls, the numerical method presented here can be extended to arbitrary axisymmetric geometries.

The mode equation for cold non-neutral plasmas is a partial differential equation which is elliptic outside the plasma and hyperbolic inside. Such problems in which the

boundary separating the two regions is an arbitrary curve are always difficult to treat.<sup>8</sup> In this paper we describe two different ways of handling this discontinuity. The first uses the cold fluid equations directly and attempts to match between the elliptic and hyperbolic regions by using a complex finite-differencing scheme near the boundary. The second uses a warm fluid model in which the sharp boundary is replaced by a diffuse one, the resulting equations are solved, and the results are extrapolated to zero temperature. Two numerical methods have been used with both models: a form of matrix shooting<sup>9</sup> and a singularity search method; both involve the direct solution of the set of equations that result from finite differencing the mode equation at every point on a grid.

When the plasma dimensions are small enough that the cylindrical walls are effectively far away, our calculations reproduce Dubin's results to within about 3%. As the plasma increases in size, two things happen. First, the plasma is no longer spheroidal in shape. It becomes more rectangular, which the calculations presented here indicate increases the mode frequencies slightly. (Note that this effect accounts for part of the 3% disagreement with Dubin's calculation; with a finite number of grid points it is difficult to remove the effect of the conducting wall.) Second, image charges in the wall reduce the perturbed electric field, which tends to decrease the mode frequencies. Neither effect is very large unless the plasma is either close to the wall or has a length longer than the cylinder diameter. For instance, for a plasma whose radius is 50% of the wall radius and whose aspect ratio (plasma half-length  $z_p$  divided by plasma radius  $r_p$ ) is less than about 3, the frequencies of the several modes studied here are only about 15% less than the mode frequencies predicted by Dubin's analysis. And since the modes in longer plasmas are described to about the same accuracy by the Trivelpiece-Gould dispersion relation, rough estimates of mode frequencies are fairly easy to make. However, using mode frequencies as diagnostics can require quite high pre-

cision, as in the work of Weimer *et al.*, where the aspect ratio was found by taking differences among closely-spaced frequencies<sup>3</sup> and in the work of Tinkle *et al.*<sup>4</sup> For such work accuracies of 10–15% are not good enough and better numerical methods like those described here are probably required. The cold sharp-boundary model discussed here seems to give accuracies in the 1–4% range while the warm-fluid model does somewhat better at 1–2%. This level of accuracy is probably not sufficient to be truly useful as a diagnostic, but might be sufficient to give useful information when used in conjunction with other diagnostic methods.

The plan of the paper is as follows. Section II discusses the mode equation and the numerical method that is used to solve it and Section III compares this method to previous calculations. Section IV discusses the effect of a conducting cylindrical wall on the mode frequencies of non-neutral plasmas, and features a table comparing the results of the rather complicated calculations of this paper with simpler calculations. It is found that for aspect ratios of 3 or higher, the Trivelpiece–Gould dispersion relation can be used in a rather simple way to find all of the numerically determined frequencies to an accuracy of 1% or better. Section V concludes the paper and the warm-fluid calculation, which is used to get zero-temperature results by extrapolation, is described in the Appendix.

## II. MODE EQUATION AND NUMERICAL METHOD

Prasad and O’Neil showed that the thermal-equilibrium density of a cold axisymmetric plasma is constant inside the plasma and zero outside the plasma, the two regions being separated by a boundary of zero thickness (sharp boundary).<sup>10</sup> They also showed a family of curves representing the shape of the boundary, which is typically not spheroidal, but conforms more to the cylindrical shape of the outer conductor. The numerical method reported here makes it possible to calculate mode frequencies for such plasmas, including the effects of nearby walls on the dynamics. We use it to find axisymmetric electrostatic drift-fluid modes in cylindrical geometry, but we are confident that it could be modified to handle other plasma models and more general geometries as well.

Prasad and O’Neil<sup>6</sup> give the drift-fluid mode equation for cold non-neutral plasmas in a uniform magnetic field parallel to the  $z$ -axis.

This model assumes that all frequencies are much less than the cyclotron frequency. For axisymmetric modes ( $m=0$ ) their equation reduces to

$$\frac{1}{r} \frac{\partial}{\partial r} \left( r \frac{\partial \phi}{\partial r} \right) + \frac{\partial}{\partial z} \left[ \left( 1 - \frac{\omega_p^2(r,z)}{\omega^2} \right) \frac{\partial \phi}{\partial z} \right] = 0, \quad (1)$$

where  $\phi$  is the wave potential, where  $\omega_p$  is the plasma frequency  $\omega_p^2(r,z) = q^2 n_0(r,z) / \epsilon_0 M$ , where  $n_0(r,z)$  is the equilibrium particle density, where  $q$  and  $M$  are the charge and mass, respectively, of the constituent particles, and where  $r$  and  $z$  are radial and axial cylindrical coordinates. Since  $n_0$  is constant inside the plasma and zero in the vacuum region, so is  $\omega_p^2$ . Thus, Eq. (1) is elliptic outside the plasma. We will see later that  $\omega^2 < \omega_p^2$  for the modes dis-

cussed here, so the  $z$ -derivative term in Eq. (1) is negative inside the plasma, making the equation hyperbolic in  $(r,z)$  inside the plasma. Thus, the equation is of mixed type, with the type change occurring along a curved boundary, making it very difficult to solve,<sup>8</sup> even with numerical methods.

The numerical solution of this mode problem proceeds as follows. We first write the finite-difference approximation to Eq. (1) at every point on a grid in  $rz$ -space, producing a set of algebraic equations that are linear in the values of  $\phi$  at the grid points. The resulting set of coupled equations has three difficulties. The first is that the linear system to be solved is singular when  $\omega$  is near a mode frequency, and near such points the accurate numerical solution of linear systems is difficult.<sup>11</sup> The second problem is that Eq. (1) is of mixed type, so standard iterative methods for solving this linear system do not converge well. These two problems are dealt with by keeping the grids as coarse as possible, by using a non-iterative banded linear system solver with high precision (which requires a lot of computer memory), and by putting up with somewhat noisy eigenfunctions. The third problem is that this is an eigenvalue problem, so the linear system is homogeneous and  $\omega$  is unknown. This problem is handled in two different ways, which will now be discussed.

### A. Two-dimensional matrix shooting

The first technique fixes the value of the wave potential at an arbitrarily chosen grid point, called the pivot point. This is done by replacing the finite-difference equation for that grid point with an equation that forces  $\phi$  at the pivot point to be one. This makes the linear system inhomogeneous, and is equivalent to choosing the amplitude of the mode. For a given choice of the mode frequency  $\omega$  the set of equations can then be solved. But for general choices of  $\omega$ , the solution has a kink at the pivot, similar to what happens to tent fabric when a pole is pushed up against it from inside. The residue  $R(\omega)$  is defined to be the finite-difference approximation to Eq. (1) evaluated at the pivot point divided by the maximum of  $|\phi|$  on the grid, and is a measure of the size of the kink. To find mode frequencies,  $\omega$  is varied until the kink disappears, as indicated by the vanishing of  $R(\omega)$ . (Note that this method is essentially the method of matrix shooting in two dimensions.<sup>9</sup>) At such values of  $\omega$  the  $\phi$  obtained by the inversion should be the wave potential of an actual mode, but in practice  $\phi$  is often rather inaccurate because it is difficult to maintain accuracy when solving a nearly-singular system. This means that frequencies are known quite a bit more accurately than are the mode eigenfunctions.

An example of  $R(\omega)$  is shown in Fig. 1. Note that the zeroes of this function cannot simply be identified by searching for sign reversals, because there are jump discontinuities that cross the horizontal axis. The reason for these discontinuities is that as  $\omega$  is varied, the structure of  $\phi$  changes, causing  $\phi=0$  curves in the  $rz$ -plane to move across the pivot point, inverting the value of the finite-difference approximation to the mode equation there. Hence, care must be taken to distinguish between sign reversals that are merely discontinuities of  $R(\omega)$  and those that indicate actual solutions of the set of finite difference equations. Some of this

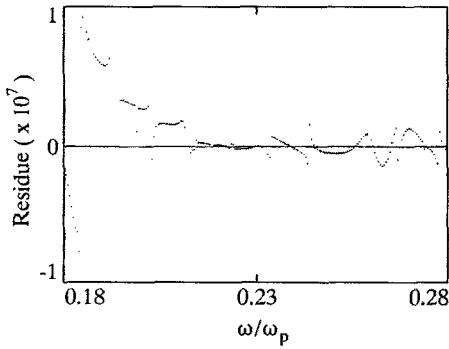


FIG. 1. Residue versus  $\omega$ . The residue is expected to vanish when  $\omega$  is the frequency of a mode. Besides the zeroes, there are also sign reversals caused by jump discontinuities. In this example, the ratio of plasma radius  $r_p$  to wall radius  $r_w$  is 0.27 and the aspect ratio  $z_p/r_p$  is 4.82. The grid has 38 radial cells and 160 axial cells in a cylindrical computation region whose radius  $r_w$  is 4.0 cm and whose length, from midplane to end-wall, is 20 cm.

can be done by careful programming, but more often it is necessary to search for zeroes on a plot of  $R(\omega)$ .

The major drawback of this method for this problem is that the spectrum of Eq. (1) is very awkward. The mode frequencies of Eq. (1) are countably infinite in number and are all confined to the interval between 0 and  $\omega_p$ . This can be seen by multiplying Eq. (1) by  $\phi$  and integrating over the interior of the conducting cylinder. After integrating by parts, the equation can be solved for  $\omega$  giving

$$\omega^2 = \omega_p^2 \frac{\int_V (\partial\phi/\partial z)^2 r \, dr \, dz}{\int [(\partial\phi/\partial r)^2 + (\partial\phi/\partial z)^2] r \, dr \, dz}, \quad (2)$$

where  $\omega_p$  is the value of the plasma frequency inside the cold plasma and where the subscript  $V$  on the integral in the numerator indicates that it is to be taken only over the volume of the plasma. The integral in the denominator is taken over the entire computing region. Modes with short radial wavelength have large average values of  $(\partial\phi/\partial r)^2$ , while modes with short axial wavelength have large average values of  $(\partial\phi/\partial z)^2$ . Thus, modes with small radial wavelength have low mode frequencies, while those with small axial wavelength have frequencies near, but just below,  $\omega_p$ . Since decreasing the axial wavelength increases the mode frequency, while decreasing the radial wavelength decreases the frequency, it is possible to find modes throughout the interval. This means that a numerical method to find the frequencies of low-order modes may also encounter other solutions of Eq. (1) with nearby frequencies, corresponding to higher-order modes.

As an example of this difficulty Fig. 2 shows a plot of the wave potential of the center-of-mass mode obtained by our numerical method for a plasma shape obtained from a numerical equilibrium calculation. [The center-of-mass mode is basically just the axial sloshing of the plasma in the electrostatic confining field. In Dubin's notation it is the (1,0) mode.] Figure 3 shows another solution of the finite difference equation which also has zero residue, obtained for the same plasma and with the same grid resolution. The frequencies of these two solutions differ only by about one part in

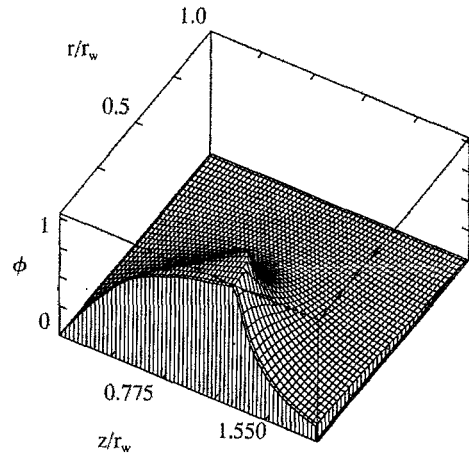


FIG. 2. The wave potential of the center-of-mass mode for a numerically computed equilibrium. We found this mode using a grid resolution of 38 radial and 160 axial cells in a computation region that is 4.0 cm in radius (axis to wall) and 20.0 cm in length (midplane to end-wall). The pivot point for the computation is close to the axis near the end of the plasma, but just inside. The plasma is 1.1 cm in radius and 5.3 cm in half-length. The frequency of this mode is  $0.230\omega_p$ . This mode potential does not look like either a Trivelpiece-Gould mode or a Dubin mode, yet the Dubin calculation obtains nearly the correct frequency ( $0.242\omega_p$ ).

two hundred. The first has the appearance of being a clear single mode, but the mode shown in Fig. 3 looks like it might be the superposition of more than one mode. In such cases, the residues associated with the different modes could be cancelling each other rather than being zeroed independently, so that neither is actually a solution of Eq. (1), or the problem might simply be a result of solving a large system of linear equations that is nearly singular. In any case the wave potential shown in Fig. 3 is probably not a good approximation to a single mode of Eq. (1).

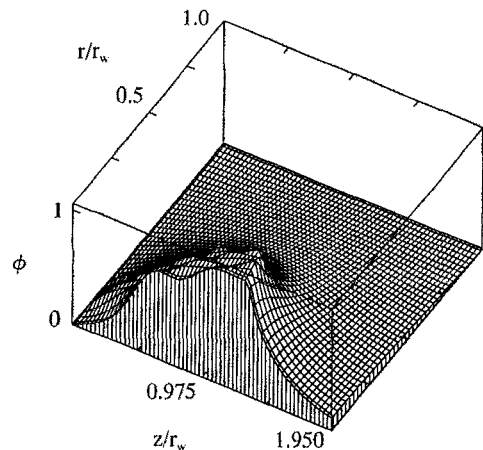


FIG. 3. A solution of the finite-difference equations with a frequency similar to that of the center-of-mass mode. Judging by its appearance, it is highly doubtful that it is a mode. This solution was obtained using the same equilibrium, pivot point, and grid resolution as the center-of-mass mode shown in Fig. 2. The frequency of this solution is  $0.231\omega_p$ .

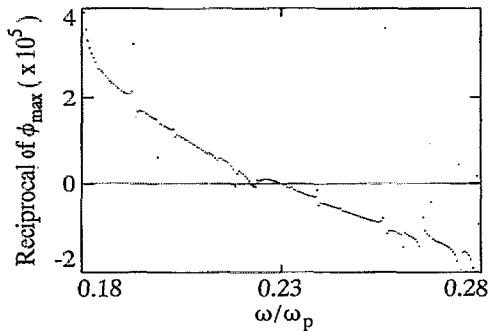


FIG. 4. The reciprocal of  $\phi$  at the point where its magnitude is largest when the right-hand side of the mode equation is taken to be  $zn_o(r,z)$  and the mode frequency  $\omega$  is scanned. Many of the modes shown in Fig. 1, though still present here, do not stand out. Among the few that do is the mode that is wanted, i.e., the center-of-mass mode at  $\omega=0.230\omega_p$ .

### B. Singularity search method

Because of the problems with the method just described, another technique was developed for dealing with the homogeneity of the set of finite difference equations. In this second technique  $\phi$  is not pinned at a pivot point, but instead the zero on the right-hand side of the set of linear difference equations for the wave potential is replaced with a rough guess at the perturbed density for a mode of interest. Since the finite-difference operator makes the left-hand side of the mode equation vanish at mode frequencies, then at these frequencies the modified equation can only be balanced by making  $\phi$  infinite. The modes are thus found by scanning the frequency  $\omega$  in a search for singularities in  $\phi$ , or equivalently, for zeroes of  $1/\phi_{\max}$  where  $\phi_{\max}$  is the perturbed potential  $\phi$  at the point where  $|\phi|$  is maximum. A plot of  $1/\phi_{\max}$  is shown in Fig. 4 for a case which has the same equilibrium as used in Fig. 1. But in producing Fig. 4, the right-hand side of Eq. (1) is replaced with a perturbed density profile that is similar in structure to (has the same number of antinodes as) the mode being sought. For example, we used this technique to find the center-of-mass mode by using  $zn_o(r,z)$  as the right hand side, i.e., the equation solved was

$$\frac{1}{r} \frac{\partial}{\partial r} \left( r \frac{\partial \phi}{\partial r} \right) + \frac{\partial}{\partial z} \left( \left[ 1 - \frac{\omega_p^2(r,z)}{\omega^2} \right] \frac{\partial \phi}{\partial z} \right) = zn_o(r,z). \quad (3)$$

The modes indicated in Fig. 1 are present here as well, but only a few stand out. Among the few are the center-of-mass mode at  $\omega=0.230\omega_p$ , which is therefore easier to find in Fig. 4 than it is in Fig. 1. (Note that the difficulty with solving a singular linear system plagues this method as well, but its effects can be reduced by careful choice of a right-hand side.) As was the case in Fig. 1, some of the discontinuities in Fig. 4 are near mode frequencies of other modes of the system. But they do not stand out because their eigenfunctions do not contribute much to the spectral content of the right-hand side chosen above. If the right-hand side were appropriately altered, these almost invisible modes could be made to stand out. Both matrix-shooting and singularity-

searching were used to obtain the results presented in this paper, but our experience suggests that singularity searching is more convenient.

### C. The sharp boundary

Another challenge is the sharp boundary of the zero-temperature plasma. To get good results it is necessary, when finite differencing at grid points near the plasma boundary, to use the value of  $\phi$  on the boundary rather than at a grid point on the opposite side of the boundary.<sup>12</sup> This requires that the value of  $\phi$  at the boundary be expressed in terms of  $\phi$  at nearby grid points, which in turn requires the use of matching conditions across the boundary. One of the plasma boundary matching conditions is that the mode potential is continuous at the plasma boundary. The other condition may be determined by integrating Eq. (1) from just inside the plasma boundary to just outside.<sup>7</sup> The resulting condition is an equation involving the  $r$ - and  $z$ -derivatives of  $\phi$  on opposite sides of the boundary. These two conditions can be combined to obtain the following jump conditions on the axial and radial derivatives of  $\phi$  at the plasma boundary:

$$\left( \frac{\partial \phi}{\partial z} \right)^+ = \left[ 1 - \cos^2 \theta \frac{\omega_p^2}{\omega^2} \right] \left( \frac{\partial \phi}{\partial z} \right)^-, \quad (4)$$

$$\left( \frac{\partial \phi}{\partial r} \right)^+ = \left( \frac{\partial \phi}{\partial r} \right)^- - \sin \theta \cos \theta \frac{\omega_p^2}{\omega^2} \left( \frac{\partial \phi}{\partial z} \right)^-, \quad (5)$$

where  $\theta$  is the angle between the outward normal to the plasma surface and the  $z$ -axis; the superscript  $+$  indicates evaluation of the derivative at a point just outside the boundary and the superscript  $-$  indicates evaluation just inside the boundary. This boundary condition is implemented by finding the crossings of the plasma boundary with the grid lines, and using these points as extra points in the calculation. At grid points neighboring the boundary, short-legged finite difference operators<sup>12</sup> are used to write the finite difference approximation to Eq. (1) in terms of the values of  $\phi$  at neighboring grid points and at points on the boundary, and the extra equations required by including the extra boundary points are obtained by interpolating on the grid to include the conditions of Eqs. (4)–(5).

A computational difficulty encountered in using this finite-difference method is that for certain grid sizes a given mode seems simply not to exist as a solution of the set of finite difference equations, caused perhaps by the rather complicated way in which we had to implement the matching conditions. In addition, because the spectrum of mode frequencies is dense in the interval  $(0, \omega_p)$ , as the grid resolution is increased, more modes are found, and they are increasingly close to each other. And, of course, the trouble caused by having to solve a nearly singular linear system is made worse as the number of grid points increases. Because of these problems we are not able to observe convergence of the mode frequency with increasing grid resolution. Instead, the mode is found for several different grid resolutions and the results are averaged. The root-mean-square (rms) deviation of the set of frequencies obtained with different grid

TABLE I. Comparison of numerical results using matrix shooting to Dubin's calculation for spheroidal plasmas with an aspect ratio of 1.5. The plasmas were chosen to have relatively small radii  $r_p$  compared to the wall radius  $r_w$ . The frequencies and error estimates were obtained by averaging across different grid resolutions.  $\ell_z$  is the number of axial nodes and  $\ell_r$  is the number of radial nodes. The principal Dubin number  $\ell$  is given by  $\ell = \ell_z + 2\ell_r$  and  $\omega_p$  is the plasma frequency in the constant density interior of the plasma.

$r_p/r_w$	Mode numbers		$\omega/\omega_p$		
	$\ell_z$	$\ell_r$	Dubin	Numerical	Relative difference
0.15	1	0	0.483	$0.477 \pm 0.002$	-0.012
0.20	2	0	0.677	$0.676 \pm 0.002$	-0.002
0.15	3	0	0.779	$0.796 \pm 0.002$	-0.02
0.15	1	1	0.253	$0.245 \pm 0.002$	-0.03
0.15	4	0	0.840	$0.838 \pm 0.001$	-0.002
0.15	2	1	0.415	$0.412 \pm 0.002$	-0.008
0.15	5	0	0.879	$0.876 \pm 0.002$	-0.003
0.15	3	1	0.530	$0.518 \pm 0.004$	-0.02

resolutions is typically seen to be about 1% for grids with about 20 to 40 radial points and 120 to 160 axial points.

#### D. Low-temperature limit of a finite-temperature fluid model

Yet another way in which we have studied these cold-fluid modes is by using the singularity-search method on the mode equation that results from adding finite temperature effects to the fluid model (see the Appendix). We use a sequence of temperatures which allow extrapolation to  $T=0$  to obtain the cold-fluid frequencies. The advantage of finite temperature is that it smooths the edge of the plasma, which eliminates the numerical difficulties caused by the sharp boundary (provided that the grid can resolve the Debye length). We find good agreement between this extrapolation method and the sharp-boundary method in most cases, but we prefer the finite-temperature method because it gives more accurate and consistent results, and is more easily extended to the rather odd equilibrium shapes which are obtained for large-radius plasmas. For example, the results in the table discussed in Section IV B were generated using this model and are internally consistent to within 1%. The results given in Section IV of the paper were obtained by means of the warm-fluid model.

### III. COMPARISON WITH OTHER CALCULATIONS

Table I compares our numerical results using the cold sharp-boundary model for spheroidal plasmas with small radii (compared to the wall radius of the trap) with results obtained from Dubin's dispersion relation in the limit of infinite cyclotron frequency. The cold-fluid model was used in making this comparison. In the table  $\ell_z$  is the number of axial nodes in the perturbed potential at  $r=0$  and  $\ell_r$  is the number of radial nodes in the potential (nodal surfaces intersecting the midplane of the plasma, other than the midplane itself). As seen in the table, Dubin's results are reproduced to within about 3%, or better, with some of the discrepancy due to the fact that the plasma was not small enough for Dubin's

calculation to be expected to apply to high accuracy. We also note that for spheroidal plasmas, the wave potentials obtained are like those calculated using Dubin's Eq. (10), except for variations on the order of less than about 10%.

We have also checked our numerical methods against a particle-in-cell code run at a low enough temperature that the equilibria had very sharp edges. (These plasmas were long enough and wide enough not to be spheroidal.) The center-of-mass mode ( $\ell_z=1, \ell_r=0$ ) in the simulation runs was excited by shifting the equilibrium density distribution slightly along the  $z$ -axis. The resulting sloshing of the plasma is mostly the center-of-mass mode (with, perhaps, harmonics) and should have the same frequency as the center-of-mass mode computed by the numerical method described here. The results indicate that the cold sharp-boundary method agrees with the simulation to within about 3% and that the warm-fluid model agrees with the simulation to within 1-2%.

These comparisons give us confidence that the method discussed here and described in Section II above is capable of examining the effects of nearby walls and of realistic equilibrium shapes on the frequencies of axisymmetric modes in non-neutral plasmas.

### IV. THE EFFECT OF A CYLINDRICAL WALL ON MODE FREQUENCIES

Of particular interest is the question of how much the frequencies of the modes calculated by Dubin are affected by image charge effects from nearby walls. This is, in general, a complicated question because it depends on the details of the conducting surfaces facing the plasma. We will focus our attention here just on the effects of a nearby cylindrical conducting wall with the end-conductors far away, but note in passing that the numerical methods discussed here can be used in general axisymmetric confining geometries.

The results of this cylindrical study are given in Table II where numerical results are compared to simpler calculations for a rather wide range of plasma radii and aspect ratios. The table was produced by using the finite-temperature model with extrapolation to  $T=0$  (see the Appendix). In the numerical calculations the computing region was taken large enough in  $z$  that the cylinder was effectively infinite. As a check on the accuracy of the values given in the table, a few of the equilibria used in the numerical computations were perturbed appropriately and fed into the particle-in-cell simulation described in Ref. 4. For the cases that were compared, the table and the simulation agreed to within about 1-2%.

To visualize the various equilibria the reader should refer to Prasad and O'Neil's paper on the subject.<sup>10</sup> Roughly speaking, when the plasma length is much less than the diameter of the cylinder, the equilibria are spheroidal, but when the plasma length is much greater than the diameter of the cylinder the plasma is cylindrical, with an end shape which varies with plasma radius. For  $r_p/r_w < 0.5$  the end of the plasma is approximately hemispherical, for  $0.5 < r_p/r_w < 0.7$  the end of the plasma is about flat (the plasma looks like a long barrel), and for  $r_p/r_w > 0.7$  the end of the plasma is concave.<sup>10</sup> For most of the entries in the

TABLE II. Comparison of numerically obtained mode frequencies with the results of simpler calculations. There are sets of mode frequencies for three different plasma radii:  $r_p/r_w=0.25$ ,  $r_p/r_w=0.50$ , and  $r_p/r_w=0.75$ . The values in the table are mode frequencies divided by the plasma frequency. The numerical results are in the column labeled "Numerical." The results in this column are accurate to the number of significant figures given, unless otherwise indicated. Each value in this column was obtained by using the warm-fluid model (see the Appendix) with four different temperatures and with extrapolation to  $T=0$ . The quoted error is the extrapolation error, which was estimated by comparing different extrapolation methods. Note that comparisons with simulations indicate an accuracy of around 1%. The column labeled "large- $\alpha$  TG fit" gives the frequencies obtained by using the Trivelpiece-Gould dispersion relation with the long-plasma  $k_{\text{eff}}$ , as described in Sec. IV B. The column labeled "Dubin" gives the frequency from Dubin's dispersion relation (no conducting walls). The column labeled "small- $\alpha$  TG fit" gives the result of choosing  $k$  so that the Trivelpiece-Gould dispersion relation with the walls far away matches Dubin's frequency, then correcting for the presence of walls, as described in Sec. IV A.

$r_p/r_w=0.25$					$r_p/r_w=0.50$						
Mode	$\alpha$	Numerical	Large- $\alpha$ TG fit	Dubin	Small- $\alpha$ TG fit	Mode	$\alpha$	Numerical	Large- $\alpha$ TG fit	Dubin	Small- $\alpha$ TG fit
(1,0)	1	.570	.509	.577	.577	(1,0)	1	.540	.529	.577	.551
(1,0)	2	.407	.392	.417	.411	(1,0)	2	.370	.373	.417	.360
(1,0)	3	.319	.316	.330	.316	(1,0)	3	.281	.283	.330	.263
(1,0)	5	.224	.225	.236	.213	(1,0)	5	.187	.189	.236	.170
(1,0)	7	.172	.173	.186	.159	(1,0)	7	.140	.141	.186	.125
(1,0)	9	.139	.140	.154	.127	(1,0)	9	.112	.112	.154	.0987
(1,0)	11	.116	.117	.132	.105	(1,0)	11	.0927	.0933	.132	.0816
(1,0)	20	.0671	.0677	.0822	.0597	(1,0)	20	.0525	.0528	.0822	.0459
(2,0)	1	.779±.006	.707	.775	.775	(2,0)	1	.783	.747	.775	.772
(2,0)	2	.612	.590	.601	.600	(2,0)	2	.612	.603	.601	.579
(2,0)	3	.510	.505	.492	.490	(2,0)	3	.497	.494	.492	.449
(2,0)	5	.388	.390	.364	.354	(2,0)	5	.352	.353	.364	.301
(2,0)	7	.313	.315	.292	.274	(2,0)	7	.270	.271	.292	.224
(2,0)	9	.260	.262	.245	.222	(2,0)	9	.218	.219	.245	.178
(2,0)	11	.223	.224	.211	.186	(2,0)	11	.182	.183	.211	.147
(2,0)	20	.132	.133	.133	.107	(2,0)	20	.104	.105	.133	.0824
(3,0)	1	.88±.02	.807	.861	.861	(3,0)	1	.881	.841	.861	.861
(3,0)	2	.727±.003	.704	.709	.709	(3,0)	2	.746	.728	.709	.702
(3,0)	3	.630	.623	.599	.599	(3,0)	3	.643	.631	.599	.577
(3,0)	5	.502	.504	.459	.455	(3,0)	5	.484	.484	.459	.410
(3,0)	7	.419	.422	.374	.364	(3,0)	7	.384	.384	.374	.312
(3,0)	9	.359	.361	.317	.302	(3,0)	9	.315	.316	.317	.250
(3,0)	11	.312	.314	.276	.256	(3,0)	11	.267	.268	.276	.208
(3,0)	20	.193	.195	.177	.150	(3,0)	20	.155	.156	.177	.117
(1,1)	1	.32±.01	.330	.340	.340	(1,1)	1	.294	.282	.340	.338
(1,1)	2	.184±.008	.183	.201	.200	(1,1)	2	.167	.164	.201	.197
(1,1)	3	.128±.002	.126	.142	.141	(1,1)	3	.117	.115	.142	.138
(1,1)	5	.078±.001	.0768	.0894	.0888	(1,1)	5	.0721	.0713	.0894	.0858
(1,1)	7	.0559	.0553	.0652	.0646	(1,1)	7	.0521	.0517	.0652	.0622
(1,1)	9	.0435	.0431	.0514	.0507	(1,1)	9	.0408	.0406	.0514	.0488
(1,1)	11	.0356	.0353	.0424	.0418	(1,1)	11	.0335	.0334	.0424	.0402
(1,1)	20	.0195	.0195	.0237	.0232	(1,1)	20	.0185	.0186	.0237	.0223

$r_p/r_w=0.75$					$r_p/r_w=0.75$						
Mode	$\alpha$	Numerical	Large- $\alpha$ TG fit	Dubin	Small- $\alpha$ TG fit	Mode	$\alpha$	Numerical	Large- $\alpha$ TG fit	Dubin	Small- $\alpha$ TG fit
(1,0)	1	.474	.478	.577	.479	(3,0)	1	.84±.02	.842	.861	.851
(1,0)	2	.310	.315	.417	.293	(3,0)	2	.704	.699	.709	.653
(1,0)	3	.228	.232	.330	.210	(3,0)	3	.577	.578	.599	.507
(1,0)	5	.149	.151	.236	.133	(3,0)	5	.411	.415	.459	.338
(1,0)	7	.111	.112	.186	.0974	(3,0)	7	.315	.319	.374	.251
(1,0)	9	.0879	.0885	.154	.0769	(3,0)	9	.253	.257	.317	.198
(1,0)	11	.0728	.0732	.132	.0635	(3,0)	11	.214	.215	.276	.164
(1,0)	20	.0411	.0412	.0822	.0356	(3,0)	20	.123	.123	.177	.0915
(2,0)	1	.730±.003	.730	.775	.741	(1,1)	1	.260	.253	.340	.321
(2,0)	2	.549±.005	.550	.601	.509	(1,1)	2	.150	.148	.201	.183
(2,0)	3	.427	.429	.492	.375	(1,1)	3	.104	.104	.142	.128
(2,0)	5	.290	.292	.364	.241	(1,1)	5	.0653	.0650	.0894	.0792
(2,0)	7	.218	.219	.292	.177	(1,1)	7	.0474	.0473	.0652	.0574
(2,0)	9	.174	.175	.245	.139	(1,1)	9	.0372	.0372	.0514	.0450
(2,0)	11	.145	.145	.211	.115	(1,1)	11	.0307	.0306	.0424	.0370
(2,0)	20	.0817	.0823	.133	.0641	(1,1)	20	.0171	.0171	.0237	.0206

table, the plasma is not spheroidal. This section of the paper will discuss the results given in the table, beginning with plasmas of low aspect ratio and finishing with plasmas of large aspect ratio. Throughout the discussion the modes will be identified by the number of axial nodes along the  $z$ -axis  $\ell_z$  and the number of radial nodes  $\ell_r$ , given in the form  $(\ell_z, \ell_r)$ . Dubin's principal mode number  $\ell$  is connected to these numbers by the relation  $\ell = \ell_z + 2\ell_r$ .

### A. Small aspect ratio

Consider first the case of low aspect ratio. When the plasma length is small compared to the wall radius the plasmas are nearly spheroidal, and we might expect Dubin's dispersion relation to give the correct mode frequencies. The entries in the table for  $r_p/r_w = 0.25$  and for  $\alpha = 1$  and  $\alpha = 2$  show that this is indeed the case. At first it might seem that the only effect of the wall would be to provide image charge, which should reduce restoring forces, and hence reduce the mode frequencies. But as can be seen from the table entries for the (2,0) and (3,0) modes at  $\alpha = 1$  and  $\alpha = 2$ , the wall has actually increased the mode frequencies slightly. The reason is that although the wall is not close enough to provide much restoring force reduction, it is close enough to flatten the equilibrium a little, making it a bit rectangular, and the numerical results indicate that "rectangularity" raises mode frequencies. This effect seems to be stronger as  $\ell_z$  increases, while image charge effects weaken as  $\ell_z$  increases (the image charges have higher multipole moments). This explains why the table entries for  $\ell_z = 1$  are below Dubin's frequency, while those for  $\ell_z = 2$  and  $\ell_z = 3$  are above it. In the corresponding table entries for  $r_p/r_w = 0.5$  and  $r_p/r_w = 0.75$  this competition between rectangularity and restoring force reduction can also be seen, with restoring force reduction winning at the largest plasma radius because the plasma is closer to the wall. These opposing tendencies make the data near  $\alpha = 1$  rather complicated.

In cases where force-reduction dominates over flattening, the effect of the wall can be estimated by using the Trivelpiece-Gould dispersion relation<sup>5</sup>:

$$\frac{I'_o(kr_p)K_o(kr_w) - K'_o(kr_p)I_o(kr_w)}{I_o(kr_p)K_o(kr_w) - K_o(kr_p)I_o(kr_w)} = \beta \frac{J'_o(\beta kr_p)}{J_o(\beta kr_p)}, \quad (6)$$

where the perturbed potential is proportional to  $\exp(ikz - i\omega t)$ , where  $K_o$ ,  $I_o$ , and  $J_o$  are the usual Bessel functions (primes indicate differentiation with respect to the function argument), and where  $\beta = \sqrt{\omega_p^2/\omega^2 - 1}$ . To make the estimate we first compute the mode frequency from Dubin's dispersion relation.<sup>7</sup> This frequency is then used in the Trivelpiece-Gould dispersion relation Eq. (6) to solve for the wavenumber  $k$  with the wall at infinity ( $r_w \gg r_p$ ). This fits the Trivelpiece-Gould dispersion relation to the correct frequency with no conducting wall. Finally, this wavenumber is used in Eq. (6) with the wall present to solve for the mode frequency  $\omega$ , approximately correcting Dubin's frequency for the presence of a conducting wall.

As an illustration of this procedure, Fig. 5. displays the center-of-mass mode (1,0) and the "breathing mode" (2,0) frequencies versus plasma radius for both the numerical computation and for the approximate Trivelpiece-Gould cal-

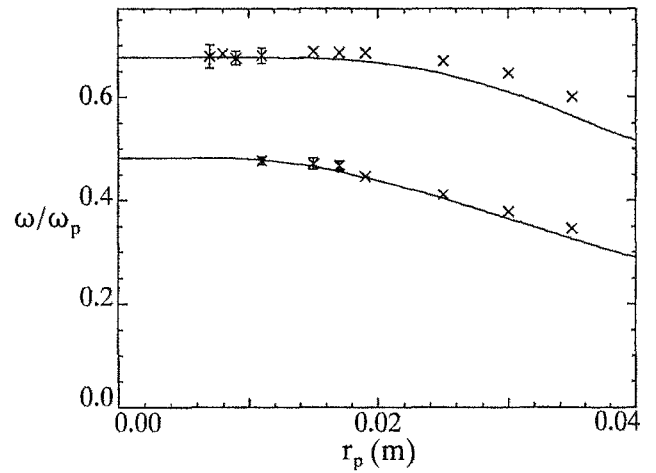


FIG. 5. Mode frequency versus plasma radius: The discrete points shown in this plot are for the center-of-mass mode (lower) and for the  $(\ell_z = 2, \ell_r = 0)$  mode (upper), for plasmas with aspect ratios of 1.5. The solid curves are Trivelpiece-Gould calculations of frequency versus radius for constant  $\lambda/z_p$ , where  $\lambda$  is the Trivelpiece-Gould wavelength, and where  $z_p$  is the half-length of the plasma of the same radius. The constant ratios  $\lambda/z_p$  are chosen to fit the Trivelpiece-Gould frequency with the wall far away to Dubin's frequencies (which can be read from the solid curves at  $r_p = 0$ ). In all these calculations, the wall radius is 4.0 cm.

ulation described above. The discrete points were obtained by using both two-dimensional matrix shooting with the cold-plasma model and singularity searching with extrapolation to zero temperature with the finite-temperature model. The plasmas all have an aspect ratio ( $z_p/r_p$ ) of 1.5. The solid curve shows the corrected Trivelpiece-Gould frequency while the data points show the results of numerical calculations. (Note that the solid curve at  $r_p = 0$  gives Dubin's frequency.) The Trivelpiece-Gould calculation gives a frequency decrease due to the presence of the conducting wall which is accurate to within about 7% for both modes, with the approximate calculation a little low compared to the numerical results in both cases. Note also that the numerical points are a little high even at small plasma radius because the wall flattens the equilibrium, as discussed above. Further examples of this procedure are given in Table II, in which the column labeled "small- $\alpha$  TG fit" gives the result of doing the calculation just described. These data suggest that for this rather simple image charge geometry and for small aspect ratios, the complicated numerical calculations can be approximated by this simpler fitting procedure, if rather poor accuracy can be tolerated.

It is, of course, also possible to interpolate directly in the table. It would be helpful in this regard to have mode frequencies at small values of  $\alpha$  for the various plasma radii, but these cases are difficult to handle with the numerical calculations presented here. One reason is that the computing region must be large enough to make the ends in  $z$  be effectively at infinity, but the grid spacing must be small enough to resolve the plasma. As the aspect ratio drops below 1, the calculation runs out of computer memory. A second problem is that the finite-temperature model runs into difficulties with acoustic resonances at low aspect ratio (see the Appendix)

which makes it difficult to find the modes. Fortunately, however, the answer at  $\alpha=0$  is easy. Dubin<sup>7</sup> shows that in the absence of conducting walls, as  $\alpha$  approaches zero all of the modes discussed here have frequencies which approach the plasma frequency. Since such plasmas are thin and are held together axially by relatively large electric fields, it might be suspected that image charge effects would be unimportant. Particle-in-cell simulations of plasmas with small aspect ratios using the same program used in Ref. 4 confirm this suspicion. And Dubin's simple result means that for interpolation purposes  $\omega/\omega_p = 1$  at  $\alpha=0$  may be added to the table, facilitating interpolation at small aspect ratios.

## B. Large aspect ratio

At large aspect ratios the plasmas become so long that they are essentially infinite in length, and it might be expected that their mode frequencies could be calculated from the Trivelpiece-Gould dispersion relation. Prasad and O'Neil showed that to lowest order in long plasmas the mode potential has an antinode at the end of the plasma, which gives the value of  $k$  to use in the Trivelpiece-Gould dispersion relation:

$$k = \frac{\pi \ell_z}{2z_p}. \quad (7)$$

The result of doing this simple calculation is approximately correct, but the convergence of this approximation to the numerical result with increasing aspect ratio is rather slow, with the difference falling off only as  $1/\alpha$ . There is, however, a better way to use the table and the Trivelpiece-Gould dispersion relation together to get a good approximation to the large- $\alpha$  portion of the table.

We begin by noting that for large  $\alpha$  the plasma looks like a cylinder with some sort of end shape, which varies with  $r_p/r_w$ . Taking a hint from the calculation of standing sound waves in an open pipe, we propose that the actual length of the plasma  $2z_p$  be replaced by an "effective length" given by

$$L_{\text{eff}} = 2z_p + \Delta L, \quad (8)$$

from which the wavenumber  $k$  may be computed for use in the Trivelpiece-Gould dispersion relation, again assuming potential antinodes at the ends:

$$k_{\text{eff}} = \frac{\pi \ell_z}{2z_p + \Delta L}. \quad (9)$$

We now assume that the end correction depends only on  $r_p$  and  $r_w$ , and estimate  $\Delta L$  by fitting to the data in Table II. It is perhaps not obvious that this will work well, and it is certainly not obvious that it will work for a simple form of the dependence of  $\Delta L$  on  $r_p$  and  $r_w$ , but in fact the simple linear form

$$\Delta L = c_1 r_w + c_2 r_p, \quad (10)$$

with

$$\begin{aligned} c_1 = 0.3; \quad c_2 = 0.7 \quad \text{for } \ell_r = 0 \quad \text{and} \\ c_1 = -0.2; \quad c_2 = 0.9 \quad \text{for } \ell_r = 1, \end{aligned} \quad (11)$$

works quite well. This choice for  $k_{\text{eff}}$  in the Trivelpiece-Gould dispersion relation reproduces all of Table II for  $\alpha \geq 3$  and for  $l_r = 0$  within 1%, or better, (even  $\alpha = 2$  is gotten within 2%) and for  $l_r = 1$  it reproduces all of the table entries to within 1%. [Note that the coefficients are not given to more significant figures than quoted above because the minimum in  $(c_1, c_2)$  space for the error between the  $k_{\text{eff}}$  fit and the table is rather broad, i.e.,  $c_1 = 0.35$  and  $c_2 = 0.65$  also does a good job of representing the  $\ell_r = 0$  data in the table.]

Note, however, that the table only deals with low-order modes (small values of  $l_r$  and  $l_z$ ), which means that  $\lambda \gg r_p$  for all of the large- $\alpha$  entries in the table, bringing up the question of how well this simple approximation works when  $\ell_z$  becomes large enough that  $\lambda \leq r_p$ . To investigate this question a few cases were tried for  $\alpha = 5$  and  $\alpha = 11$  with values of  $\ell_z$  ranging up to 33. It is found that the simple approximation continues to work to about 1% accuracy, greatly facilitating the calculation of mode frequencies of cold non-neutral plasmas in cylindrical geometry.

## C. Potential as a diagnostic

Table II can be used to assess the potential of this calculation as a plasma diagnostic. A cold plasma in global thermal equilibrium inside a conducting cylinder is completely characterized by three parameters: density  $n_o$ , midplane radius  $r_p$ , and half-length on axis  $z_p$ . The dependence on  $n_o$  can be eliminated by taking ratios between frequencies in the table, say  $\omega_{20}/\omega_{10}$  and  $\omega_{30}/\omega_{10}$ . A table of these ratios as a function of  $r_p$  and  $z_p$  might then be used to look up experimentally measured frequency ratios to determine the radius and half-length. When such a table is constructed from the data in Table II it is clear that there is not enough variation of the frequency ratios with  $r_p$  to make a calculation with an accuracy of 1–2% give useful information about plasma shape. The calculation would have to be more accurate by about an order of magnitude to be useful in this sense. If, however, the radius were determined in some other way (say by dumping the plasma out of the trap onto charge collectors), a calculation of this kind could give valuable information about length and density, especially if it were an order of magnitude more accurate. Plasmas of experimental interest are not necessarily in global thermal equilibrium nor are they at  $T=0$ . So in addition to these three parameters, radial profile and temperature must also be determined, indicating that the value of a calculation of this kind might be to provide additional information to be used in conjunction with already existing diagnostic methods. For example, the warm-fluid method described here gives the same information about plasma temperature (to within 1%) as the simulation discussed in Ref. 4, but is much faster.

## V. CONCLUSION

We have numerically solved the mode equation for cold non-neutral plasmas in a conducting cylinder including the effect of realistic equilibrium shape by using a two-dimensional version of matrix shooting and also by looking for the singular values of the linear system obtained from the finite-difference approximation to the mode equation. A

rather extensive table of mode frequencies for various modes and for many plasma shapes is given. For plasma aspect ratios below about 2 a combination of Dubin's calculation and the Trivelpiece-Gould dispersion relation is found to give approximately correct results, while for aspect ratios above 3 a simple approximation method is found which uses the Trivelpiece-Gould dispersion relation to obtain the numerically-computed values to within about 1%. Finally, a calculation of this kind which included finite-temperature and general radial profiles might be useful as a diagnostic if the accuracy could be improved by about an order of magnitude.

## ACKNOWLEDGMENTS

The authors are grateful for useful discussions with Grant Hart, Grant Mason, Neil Rasband, and with the referees. Special thanks go to Robert Jones for developing and running the particle simulation code against which the results reported here were tested, and to group T-15 at Los Alamos National Laboratory and to the Department of Physics at the University of California at San Diego.

## APPENDIX: WARM FLUID MODEL

In this appendix the finite-temperature model is described. It assumes drift motion perpendicular to a uniform confining magnetic field in the  $z$ -direction and an adiabatic fluid response parallel to the confining field. Only electrostatic effects are included. The fluid equations (unperturbed) corresponding to this description are

$$\frac{\partial n}{\partial t} + \mathbf{v}_d \cdot \nabla n + \frac{\partial}{\partial z}(n v_z) = 0, \quad (\text{A1})$$

$$\mathbf{v}_d = \frac{-\nabla \phi \times \hat{z}}{B}, \quad (\text{A2})$$

$$Mn \left[ \frac{\partial}{\partial t} v_z + \mathbf{v} \cdot \nabla v_z \right] = -qn \frac{\partial \phi}{\partial z} - \frac{\partial p}{\partial z}, \quad (\text{A3})$$

$$\frac{\partial p}{\partial t} + \mathbf{v}_d \cdot \nabla p + v_z \frac{\partial p}{\partial z} = -\gamma p \frac{\partial v_z}{\partial z}, \quad (\text{A4})$$

$$\nabla^2 \phi = -\frac{q}{\epsilon_0} n, \quad (\text{A5})$$

where  $n$  is the particle density,  $\mathbf{v}_d$  is the drift velocity perpendicular to the magnetic field  $\mathbf{B}$ ,  $v_z$  is the fluid velocity parallel to  $\mathbf{B}$ ,  $\phi$  is the electrostatic potential,  $M$  is the particle mass,  $q$  is the particle charge,  $p$  is the fluid pressure parallel to  $\mathbf{B}$ , and where  $\gamma$  is the adiabatic exponent, which we take to be 3 because the strong magnetic field limits the kinetic response of the plasma to just one dimension.

When these equations are linearized to describe small perturbations about a non-neutral plasma equilibrium described by unperturbed density  $n_o = n_o(r, z)$  and unperturbed electrostatic potential  $\phi_o = \phi_o(r, z)$  the following mode equation for the perturbed potential  $\phi$  results [ $\phi(r, z, \theta) \rightarrow \phi(r, z) \exp(im\theta - i\omega t)$ ]:

$$\begin{aligned} & \gamma \lambda_D^2 \frac{\partial}{\partial z} \left[ V \frac{\partial}{\partial z} \nabla^2 \phi \right] + \gamma \lambda_D^2 \frac{\partial}{\partial z} \left[ V \frac{\partial F_o}{\partial z} \nabla^2 \phi \right] \\ & - \frac{(\gamma-1) m v_{th}^2}{r \omega_c} \frac{\partial}{\partial z} \left[ V \frac{\partial}{\partial z} \left( \frac{\partial n_o / \partial r}{n_o (\omega - m \omega_o)} \phi \right) \right] \\ & - \frac{(\gamma-1) m v_{th}^2}{r \omega_c} \frac{\partial}{\partial z} \left[ V \frac{\partial F_o}{\partial z} \frac{\phi}{(\omega - m \omega_o)} \right] \\ & + \frac{(\omega - m \omega_o)}{\omega_p^2} \nabla^2 \phi - \frac{\partial}{\partial z} \left[ V \frac{n_o}{n_o} \frac{\partial \phi}{\partial z} \right] - m \frac{\partial n_o / \partial r}{r \omega_c n_o} \phi = 0, \end{aligned} \quad (\text{A6})$$

where  $\lambda_D$  is the Debye length obtained from the central equilibrium density  $n_{oo}$ ,  $kT$  is the temperature (assumed independent of  $r$  and  $z$ ) in energy units,  $F_o = q \phi_o / kT$ ,  $v_{th} = \sqrt{kT/M}$  is the thermal speed,  $\omega_c$  is the cyclotron frequency, and where  $\omega_o = \omega_o(r, z) = v_d / r$  is the drift rotation frequency. The quantity  $V$  which appears throughout the equation is given by

$$V(r, z) = \left[ \omega - m \omega_o + (\gamma-1) v_{th}^2 \frac{\partial}{\partial z} \left( \frac{\partial F_o / \partial z}{(\omega - m \omega_o)} \right) \right]^{-1}. \quad (\text{A7})$$

It is perhaps worth noting that this mode equation in infinitely-long geometry works very well, giving essentially the same dispersion relation as the corresponding kinetic-theory calculation until the phase velocity becomes comparable to the thermal velocity and Landau damping becomes important. The mode equation is given for arbitrary azimuthal mode number  $m$  for completeness, but in the work described in this paper  $m=0$ , which simplifies it considerably. Note also that as the temperature approaches zero only the last three terms in Eq. (A6) survive and  $V=1$ , recovering the cold mode equation given by Prasad and O'Neil.<sup>6</sup>

This mode equation is solved by finite-differencing in the usual way, and then using the singularity search method described in Section II. Adequate accuracy (1%) requires that the grid spacing in both  $r$  and  $z$  be less than, or about equal to, the Debye length. As a test, this model was used on the equilibria from which the simulation results reported in the paper by Tinkle *et al.*, were obtained.<sup>4</sup> The frequencies from the warm fluid calculation were within 2% of the simulation results, even though the Debye length was large enough that kinetic effects were beginning to be significant.

To use this calculation to obtain results at zero temperature, a singularity search calculation is carried out on several different equilibria with the same external confining potentials but with different temperatures. In the study described here the equilibria are global thermal equilibria.<sup>10</sup> The resulting pairs of temperatures and frequencies are then used to extrapolate the frequency to zero temperature. This means that it should also be possible to give the variation of frequency with temperature, but for many of the cases there was so little change of frequency with temperature that the variation was difficult to compute with any accuracy. Finite temperature results will be discussed in a later paper. The procedure works very well for plasmas which are rather rectangular, but for spheroidal plasmas, and especially for

spheroidal plasmas of small aspect ratio, acoustic resonances creep in which spoil the calculation unless very small temperatures (and hence very fine grids) are used. These effects will also be discussed in detail in a subsequent paper.

<sup>1</sup>J. H. Malmberg and J. S. deGrassie, *Phys. Rev. Lett.* **35**, 577 (1975).

<sup>2</sup>R. C. Davidson, *Physics of Non-neutral Plasmas* (Addison-Wesley, Redwood City, CA, 1990).

<sup>3</sup>C. S. Weimer, J. J. Bollinger, F. L. Moore, and D. J. Wineland, *Phys. Rev. A* **49**, 3842 (1994).

<sup>4</sup>M. D. Tinkle, R. G. Greaves, C. M. Surko, R. L. Spencer, and G. W. Mason, *Phys. Rev. Lett.* **72**, 352 (1994).

<sup>5</sup>A. W. Trivelpiece and R. W. Gould, *J. Appl. Phys.* **30**, 1784 (1959).

<sup>6</sup>S. A. Prasad and T. M. O'Neil, *Phys. Fluids* **26**, 665 (1983).

<sup>7</sup>D. H. E. Dubin, *Phys. Rev. Lett.* **66**, 2076 (1991).

<sup>8</sup>J. M. Rassias, *Lecture Notes on Mixed Type Partial Differential Equations* (World Scientific, Teaneck, NJ, 1990), p. 137.

<sup>9</sup>J. P. Freidberg and D. W. Hewett, *J. Plasma Phys.* **26**, 177 (1981).

<sup>10</sup>S. A. Prasad and T. M. O'Neil, *Phys. Fluids* **22**, 278 (1979).

<sup>11</sup>W. H. Press, S. A. Teukolsky, W. T. Vetterling, and B. P. Flannery, *Numerical Recipes* (Cambridge University Press, Cambridge, 1992), p. 47.

<sup>12</sup>G. D. Smith, *Numerical Solutions of Partial Differential Equations* (Oxford University Press, London, 1965), p. 139.